Surface & Coatings Technology 337 (2018) 241–249

Contents lists available at ScienceDirect

Surface & Coatings Technology

journal homepage: www.elsevier.com/locate/surfcoat

Development of long laminar plasma jet on thermal spraying process: Microstructures of zirconia coatings

Sen-Hui Liu[a], Cheng-Xin Li[a,*], Lu Li[b], Jia-Hua Huang[b], Pan Xu[b], Ying-Zhen Hu[a], Guan-Jun Yang[a], Chang-Jiu Li[a]

[a] State Key Laboratory for Mechanical Behavior of Materials, School of Materials Science and Engineering, Xi'an Jiaotong University, Xi'an, Shaanxi 710049, China
[b] Zhenhuo Plasma Technology Company, Chendu, Sichuan 610065, China

ARTICLE INFO

Keywords:
Laminar plasma jet
Thermal spraying
YSZ coatings
Vertical cracks
Thermal conductivity

ABSTRACT

A novel direct current non-transferred arc plasma torch that can generate long, silent and stable laminar plasma jet in air is applied to thermal spraying process in this article. Such long laminar plasma jet, making a low level of noise (< 80 dB) in air, features a jet length over 350 mm, and presents regular variation in length with the increase of output power and gas flow rate. Microstructures and properties of YSZ coatings obtained under spraying distances ranging from 130 mm to 300 mm are discussed in the following. The results show different intervals of vertical cracks across the transverse sections of the coatings and orderly distributed island-protrusions on the top surface of the coatings. A mass of vapor deposited structures can be found in the samples, that means the refractory 8YSZ powders can be melted sufficiently when flowing in long laminar plasma jet, although the stable output power of the laminar plasma torch is only 25–26 kW during the spraying process. This may provide extensive options for different plasma spraying applications and improve the controllability of plasma spraying technology.

1. Introduction

Thermal plasma spraying technology can deposit many functional coatings, like temperature or wear resistant coatings, electrically conductive or insulative coatings. Technically, in a conventional non-transferred arc plasma torch, the arc is operated across a flow of argon, hydrogen, helium, nitrogen or mixtures between a cathode and a nozzle-shaped water-cooled anode where the plasma gas is induced along the cylindrical channel and injected into atmospheric environment [1]. Then fine metallic or ceramic powders suspended in carrier gas are injected into the thermal plasma plume in radial or axial direction, where solid powders are accelerated and heated to molten or semi-molten state. Finally, these particles unceasingly impinge on the prepared substrate to form numerous overlapped lamellae that constitute more or less dense coatings. It is the well-established atmospheric plasma spraying process that has been much investigated and widely used in plasma processing industry. However, the lengths of plasma jets generated by the conventional plasma torches never exceeded 200 mm in atmospheric environment [2], the spraying distance is always in the range of 80 mm ~ 150 mm. This plasma generation equipment also makes a huge noise around the workbench, usually 120–130 dB [3,4]. The working power and gas flow rate of this conventional plasma equipment usually exceed 30 kW and 40 slpm, respectively [4]. For example, the overall argon-based plasma jet from the non-transferred arc plasma torch in air is probably less than one-third argon due to the rapid entrainment of the surrounding gas [5]. It is unfeasible to precisely control the heating and motion of particles in the plasma plume due to the rapid cold air mixing of the jet and high axial velocity or temperature gradients, especially for oxygen-sensitive metals or refractory materials.

In order to improve the controllability and reproducibility of the plasma spraying process, a specially designed direct current non-transferred arc plasma torch with serial interelectrode inserts between the anode and the cathode can generate a kind of silent, stable and long laminar plasma jet in air, which means that the plasma jet length and relative flow field characteristics can be conveniently controlled through the gas flow rate and the output power of the equipment. Until now, several pioneer researchers from institutes all over the world have been working on these high-enthalpy or laminar non-transferred arc plasma torches, as listed in Table 1. The output power of laminar

Abbreviations: SEM, scanning electron microscopy; XRD, X-ray diffraction; SPPS, solution precursor plasma spray; APS, atmospheric plasma spray; YSZ, yttria stabilized zirconia

* Corresponding author at: School of Materials Science and Engineering, Xi'an Jiao tong University, State Key Laboratory for Mechanical Behavior of Materials, Xi'an, Shaanxi 710049, China.
E-mail address: licx@mail.xjtu.edu.cn (C.-X. Li).

https://doi.org/10.1016/j.surfcoat.2018.01.003
Received 8 July 2017; Received in revised form 31 December 2017; Accepted 2 January 2018
Available online 03 January 2018
0257-8972/

Table 1
The main research history of laminar plasma torches.

Year	Departments	Authors	Working power/gas	Nozzle diameter/jet length
1995	Institute of Theoretical and Applied Mechanics, Russia Academy of Sciences [6]	Mikhail F. Zhukov, Solonenko, O.P et al.	50 kW Ar + 3%H_2	D = 8 mm, L = 500 mm
1997	Institute of Aeronautical Engineering, Aviation Industry of China [7].	H.C. Wu; X.D. Yang	Ar, 13–14 L/min 17.4 kW	L = 100–500 mm
2000	Yamaguchi University, Japan [8].	Osaki, K et al.	Ar, 5–8 L/min 2.35–3.43 kW	D = 6 mm, L = 400–450 mm
2001	Nippon Steel Corporation, Japan [9].	Hideki Hamatanis et al.	Ar + 2%N_2 18–40 kW	D = 18 mm, L = 600 mm
2001	Institute of Mechanics, Chinese Academy of Science, China [10].	W.X. Pan, C.K. Wu et al.	Ar/Ar + N_2, 12–30 L/min 15–30 kW	D = 4–10 mm, L = 250–600 mm
2008	Ashikaga Institute of Technology, Japan [11].	Yasutaka Ando. et al.	Ar, 3.5–10 L/min, 3.12 kW	D = 6 mm L = 100 mm
2008	Georgian Technical University, Georgia [12].	M. Khutsishvili	Ar 7.5–9 kW	D = 7–8 mm L = 140 mm
2012	Xi'an Institute of Optics and Precision Mechanics, Chinese Academy of Science [13].	Tang, J. et al.	N_2 500 W (DC Glow Discharge)	D = 15 × 1 mm (rectangle) L = 15 mm
2014	University of Limoges, France [14].	J. Krowka et al.	N_2, 1.1 kW 0.0336–0.0992 L/min	D = 2.5–4 mm L = 10–14 mm
2015	Sichuan university, China [15,16].	De-ping Yu et al.	N_2/Ar, 1.3–4.1 L/min 0.9–10 kW	D = 3 mm L = 300–400 mm
2015	University of Science and Technology of China, China [17]	Jiang-ling Wang, Z. X. Dong et al.	N_2/Ar, 5–8.5 L/min 1.2–5 kW	D = 3–5 mm L = 180–500 mm

plasma equipment varied from 2.35 kW to 50 kW, anode nozzle diameters from 4 mm to 18 mm, and the plasma jet length from 100 mm to 600 mm.

These types of laminar plasma torches have been successfully used in three-dimensional additive manufacturing [17], plasma synthesis of fine powders [18,19], welding [20], remelting or cladding of metallic surfaces [21,22] and demonstrated exceptional performances. Nevertheless, studying of laminar plasma deposition of coatings is in the initial research stage and a few papers focus on the characteristics of laminar plasma sprayed coatings [23,24,25,26]. The disadvantages and advantages of applying the laminar plasma jet on material spraying process should be studied. Furthermore, the influences of using laminar plasma jet on formation and performances of coatings need to be researched systematically. Therefore, in this article, a novel laminar plasma torch that can also generate long, silent and stable laminar plasma jet in ambient air was applied in the framework of thermal spraying technology. Microstructures and physical performances of YZS coatings deposited at the spraying distance ranging from 130 mm to 300 mm were discussed in this paper.

2. Experimental methods

2.1. Processing and materials

All YSZ coating experiments were carried out on the novel long laminar plasma spraying system (ZH-30, Zhenhuo Plasma Technology Company, Chengdu, China), which can generate different lengths of laminar plasma jet under a wide range of output powers and gas flow rates, making a low-level noise (< 80 dB) in ambient environment. The laminar plasma jet length presented rich variation with the increase of working current ranging from 60 A to 165 A under every given gas flow rate from 8.5 L/min to 15 L/min. This may provide wide options for different plasma spraying processing. A schematic diagram of the laminar plasma spraying process was showed in Fig. 1, more details of working parameters were listed in Table 2. The rated power of the equipment was 30 kW, the stable output power was 25–26 kW during the experiment. Generally speaking, in conventional plasma spraying, the optimal spraying distance between the torch nozzle and the substrate is typically 80 mm to 150 mm, depending on the arc current, plasma gas flow rate and spray materials. In this article, a super-long spraying distance ranging from 130 mm to 300 mm was realized by using this laminar plasma jet.

8% yttria stabilized zirconia powder (Metco 204 B-NS, −75∼+39 μm, Sulzer Metco, Westbury, USA) was used as the feedstock material (Fig. 2), and other processing conditions remained constant for all runs. The particle injection in this case was through a specific gravity-vibration device in the radial direction, and did not use the conventional powder supply by the way of auxiliary gas, as the auxiliary gas at the nozzle exit can perturb the flow stability of this laminar plasma jet. The initial injecting velocity was < 3 m/s at the mass flow rate of 3 g/min.

The substrate used in coating deposition was 304 stainless steel, which was prepared after grit-blasting, with a NiCoCrAlY bond coating having a thickness of 100 μm and roughness of 10–15 μm deposited by a low-pressure plasma spraying (LPPS) system (Ni23Co20Cr8.5Al4.0Ta0.6Y, Amdry 997, −37 ∼ +9 μm, Sulzer Metco, Westbury, NY) [27]. The long laminar plasma jet must be perpendicular to the sample. The sample holding device can be cooled by circulating water or gas.

2.2. Characterization of coating microstructure

The microstructure morphologies of YSZ coatings were characterized by a scanning electron microscope (SEM, VEGA II, TESCAN, Czech). The phase constituents were identified by X-ray diffraction (XRD, Rigaku D/max 2400). The porosity of the coatings was determined by image analyzing method using scanning electron microscope images of the polished cross sections. At least ten images were used to estimate the apparent porosity for each coating sample. The hardness of the coatings was measured on the polished cross sections of coatings with a Micro Vickers Hardness Meter with a load of 300 gf and a holding time of 10 s (10 different positions for each sample, BUEHLER MICROMET5104, Akashi Corporation, Japan). Keyence color 3D laser scanning microscope (VK-9700, violet laser) was operated to measure the top surface roughness of the coatings.

2.3. Measurement of thermal conductivity of coatings

The thermal conductivity is calculated by Eq. (1):

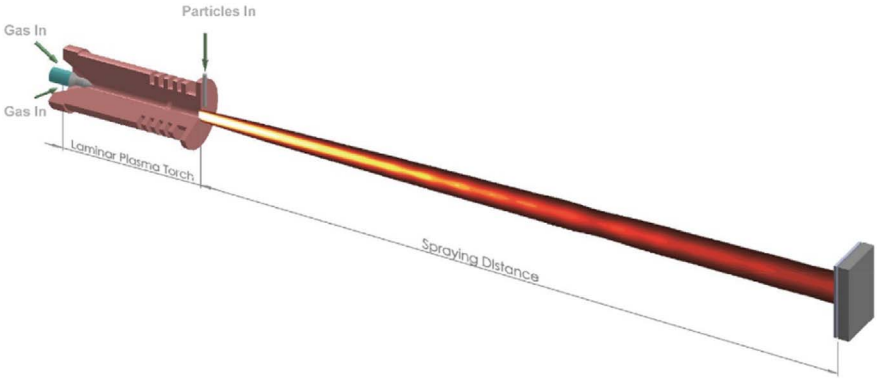

Fig. 1. Schematic diagram of laminar plasma spraying process.

Table 2
Laminar plasma spraying parameters.

Parameters	Value
Input power/kW	25–26
Torch move velocity/m/s	0.4
Torch move interval/mm	4
Spraying distance/mm	130–300
Plasma gas N_2/Ar	7:3 (by volume)
Flow rate of working gas/slpm	14
Feedstock	8YSZ (Metco 204 B-NS)
Powder feed rate/g min^{-1}	3–4 (no carrier gas)

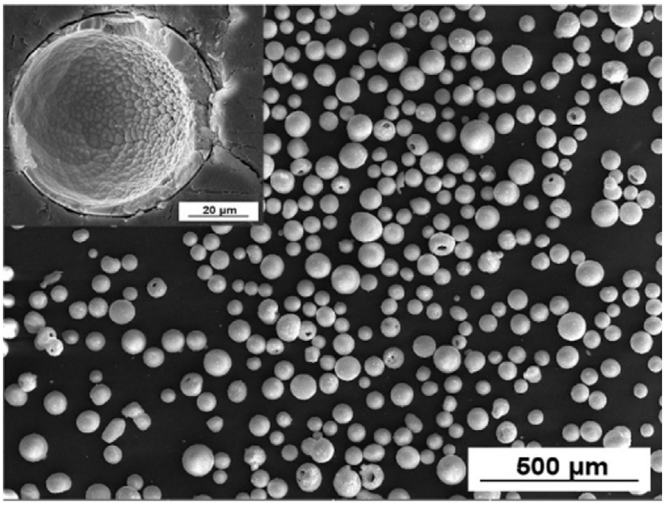

Fig. 2. Morphology of the hollow and spherical 8YSZ powder used for top coating.

$$\lambda = \alpha \cdot C_p \cdot \rho \quad (1)$$

where α is the thermal diffusivity, C_p is the specific heat capacity, ρ is the density, and λ is the thermal conductivity [28,29]. The thermal diffusivities (α) of the YSZ coatings were measured using a laser-flash apparatus (Netzsch, LFA-427) from 298 K to 1273 K. The surfaces of the specimens were coated with a thin film of graphite for thermal absorption of laser pulses at the beginning. Each sample was measured three times at one selected temperature. The value of the heat capacity of the coatings was determined with differential scanning calorimeters 404 (Netzsch, Germany). The density of the coatings was calculated through dividing the mass with the volume of the test sample. The diameter of the coatings was designed as 12.7 mm–13 mm, these were separated away from the substrate by dilute hydrochloric acid solution.

3. Experimental results

3.1. Generation of the long laminar plasma jet

The laminar plasma equipment used in this work can generate long, stable and silent laminar plasma jet in ambient air by using nitrogen and argon working gases, showing regular variation in plasma jet length under every given gas flow rates or output power and making a relatively low level of noise (< 80 dB) in ambient environment. Fig. 3 shows the voltage-current characteristic of the supply power and the variation of plasma jet length at different output powers at a constant gas flow rate of 14 L/min. The jet length is increased with the increase of output power. The maximum jet length in air can reach about 360 mm at the working current of 160 A and the gas flow rate of 14 L/min. Fig. 4 shows the 8YSZ particles, density of 5.85 g/cm^3, as they are heated and accelerated in the long laminar plasma jet in air (Nikon D3400). The initial injecting velocity of particles was < 3 m/s, a super-long acceleration time and heat transfer distance can be acquired in this experiment when particles flow in the laminar plasma plume.

3.2. Comprehensive microscopic observation of YSZ coatings obtained under different operation conditions

This section elaborates the comprehensive microstructure views of YZS coatings under five different spraying distances using this laminar plasma torch in ambient air, as specified in Table 3. Observations include fracture surfaces, top surfaces and polished cross-section surfaces (Figs. 5–9). The minimum thickness of the coatings was over 200 μm. There also existed different densities of vertical segmentation cracks along the transverse section of the five coatings. Besides, small

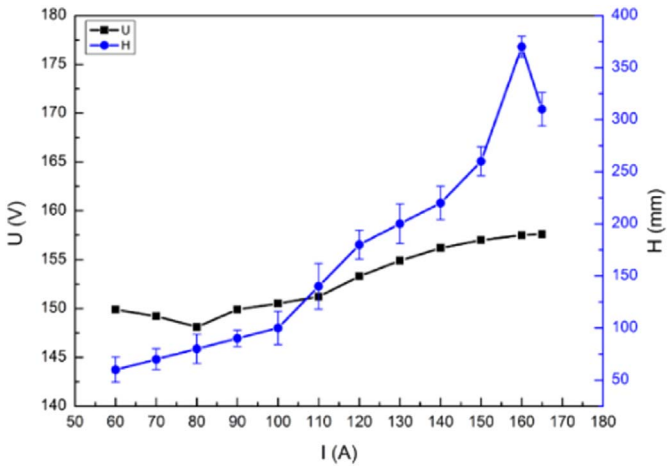

Fig. 3. Voltage-current characteristics and dependence of laminar plasma jet length at the gas flow rate of 14 L/min (N_2:Ar = 7:3 by volume).

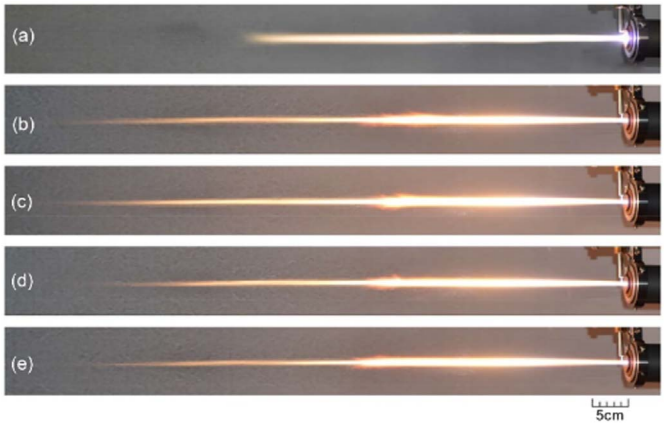

Fig. 4. Photos of laminar plasma jet without particles (a) and with particles heating and acceleration over four consecutive seconds, after 1 s (b); 2 s (c); 3 s (d) and 4 s(e).

Table 3
Spraying parameters of five coatings.

Sample	Spraying distance/mm	Thickness/μm	Working current/A	Working voltage/V
A	130	200 ± 15	160	157.5
B	180	210 ± 10	160	158.0
C	220	200 ± 10	160	158.0
D	250	200 ± 10	160	157.7
E	300	210 ± 20	160	157.6

horizontal branched cracks, growing from the vicinity of larger vertical cracks, can also be detected. In this experiment, at these super-long spraying distances ranging from 130 mm to 300 mm, ceramic coatings can also be deposited by this novel laminar plasma torch in air, which is unfeasible by conventional plasma spraying equipment.

Fig. 5 is related to the microstructure of the coating deposited at the spraying distance of 130 mm by this novel laminar plasma torch. The spraying distance of 130 mm is common to other conventional plasma torches. The polished transverse section of coating presented a porous microstructure with more voids compared to other specimens (Fig. 5-c, d); the top surface of the coating was characterized by the mean roughness of 22.4 μm and consisted of overlapped splats (Fig. 5-a, b). The fracture section demonstrated a typical lamellar structure composed of numerous solidified flat particles which was much familiar to the conventional atmospheric plasma sprayed coatings (Fig. 5-e). The specimen had a size of 50 mm × 80 mm, eight robot cycles with a scanning velocity of 0.4 m/s and move interval of 4 mm are enough to obtain a coating with thickness of 200–220 μm at a powder feed rate of 3–4 g/min, where the powder did not fly around because the laminar plasma jet produced a very focused deposition spot onto the substrate, and there was no need for other auxiliary dust collection devices during the spraying process.

Figs. 6 and 7 demonstrated sample B and C with high segmentation crack density of 4 cracks per millimeter, and smaller parallel cracks were linked to the larger vertical cracks in the polished transversal section. Besides, it was a remarkable phenomenon that several island-protrusions were orderly distributed at the top surface of the coating from the lower and higher magnification views of the top surface SEM images (Figs. 6-a, b and 7-a, b), and it was also a noticeable feature that the inclination direction of those island-protrusions was in accordance with the robot-scanning pass direction, which meant the spraying direction of these coatings was from left to right in Figs. 6-a and 7-a. The tip of every island-protrusion was the aggregation of vapor deposited villous structures with mean diameter of 2.5 μm and without clearly unmelted particles in SEM views (Figs. 6-c and 7-c). At the spraying distance of 180 mm to 220 mm, the 8YSZ powders, melting point of 2953 K and boiling point of 4573 K [30], were mostly melted into droplets and even vaporized under such super long heating distance,

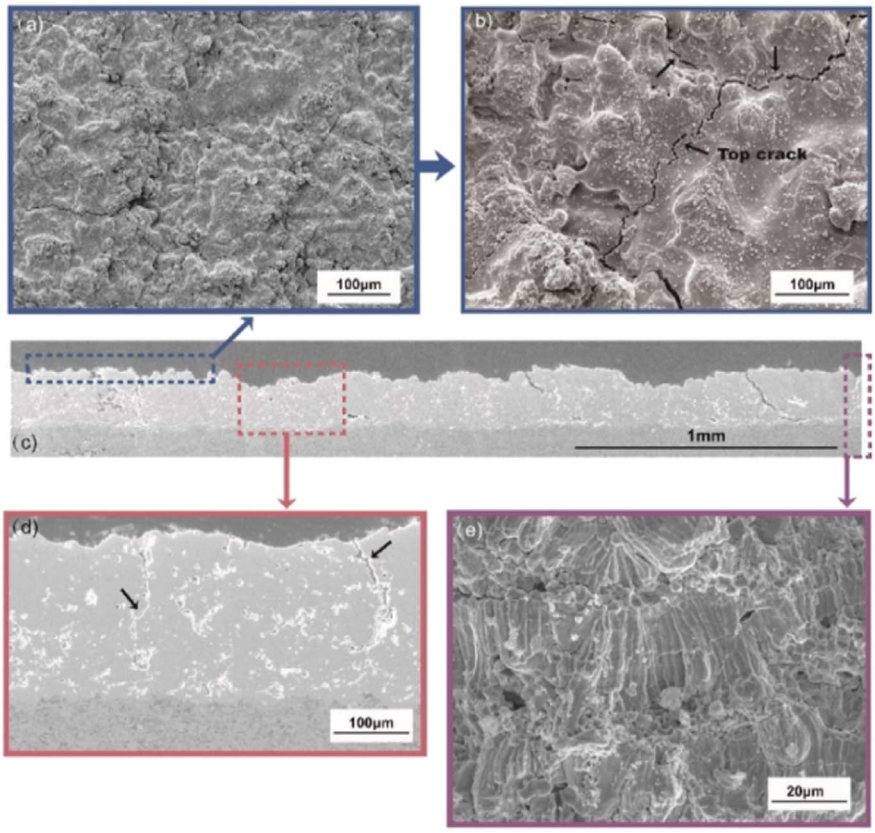

Fig. 5. Top surface (a, b), cross section (c, d) and fracture surface (e) of YSZ coatings at the spraying distance of 130 mm (sample A).

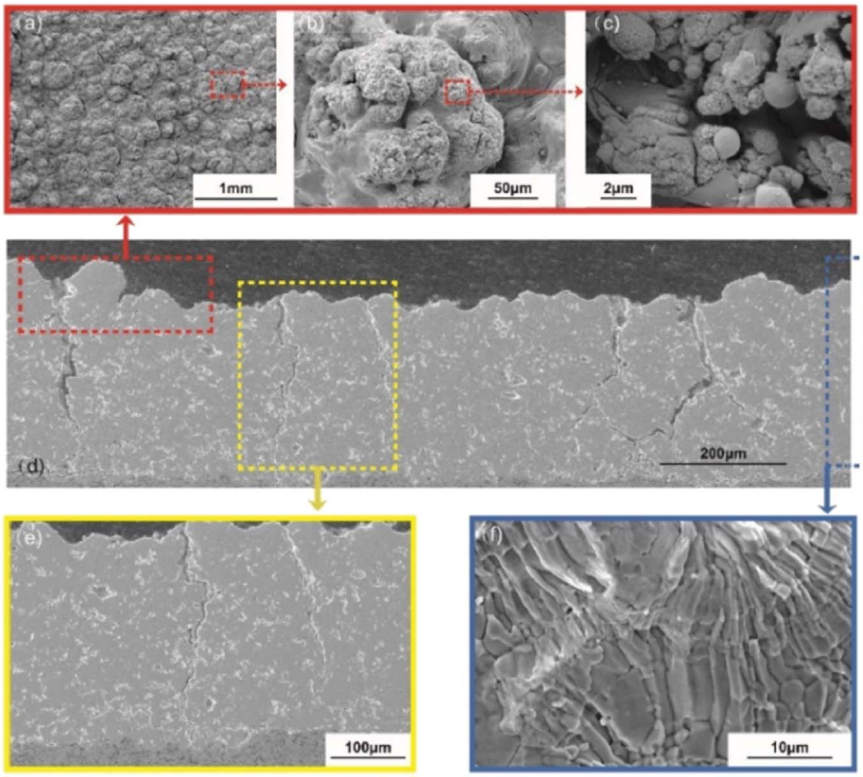

Fig. 6. Top surface (a, b, c), cross section (d, e) and fracture surface (f) of YSZ coatings at the spraying distance of 180 mm (Sample B).

then they impinged on the substrate and solidified to form lamellar structures as shown in the fracture sections (Figs. 6-f and 7-e). The sub-micro sizes of voids or pores on the cross sections were much smaller than the height of top protrusions (> 30 μm) from the observations of top surfaces and the size of lamellas (1–2 μm) from the observations of fracture surfaces. As the later generated droplets in the laminar plasma jet overlaid the previous ones, and flattened well, they resulted in the formation of the lamellar structure, and of course, penetrated and filled the gaps around the island-protrusions eventually.

At the spraying distance of 250 mm (Fig. 8), small branched cracks and larger vertical cracks also existed along the transverse section of coating (Fig. 8-e). The polished transversal surfaces of the coating show porous-layered structure and overlapped lamellas exhibiting a good bonding with unclear splat boundaries, which were very familiar to other solution-precursor plasma sprayed YSZ coatings [31,32]. Fewer vapor deposited areas, comparing with Sample B and C (Figs. 6-c and 7-

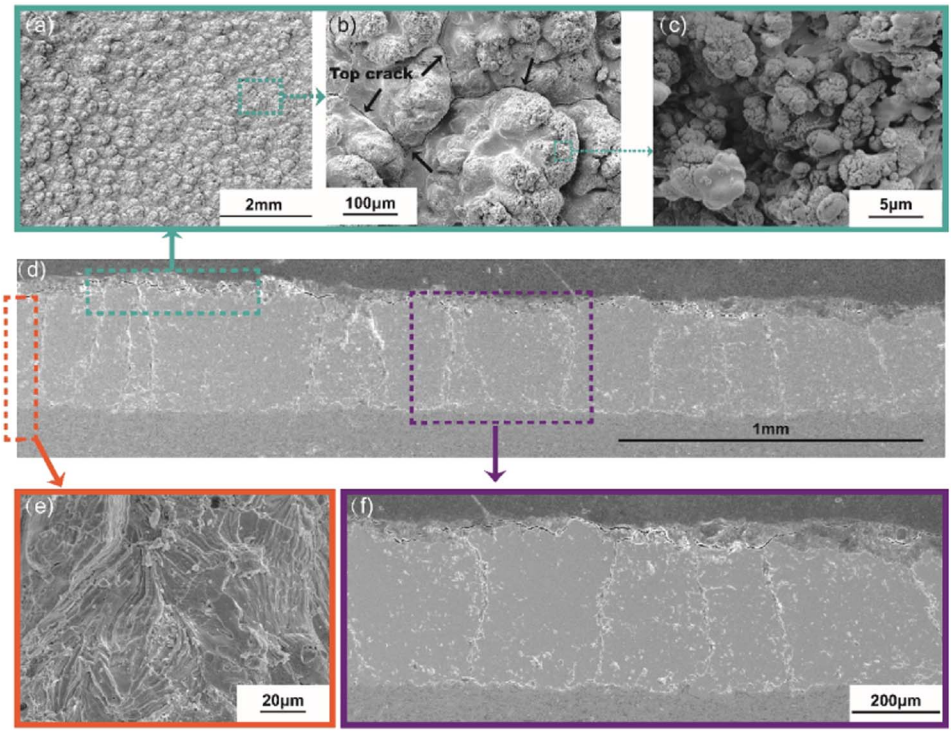

Fig. 7. Top surface (a, b, c), cross section (d, f) and fracture surface (e) of YSZ coatings at the spraying distance of 220 mm (Sample C).

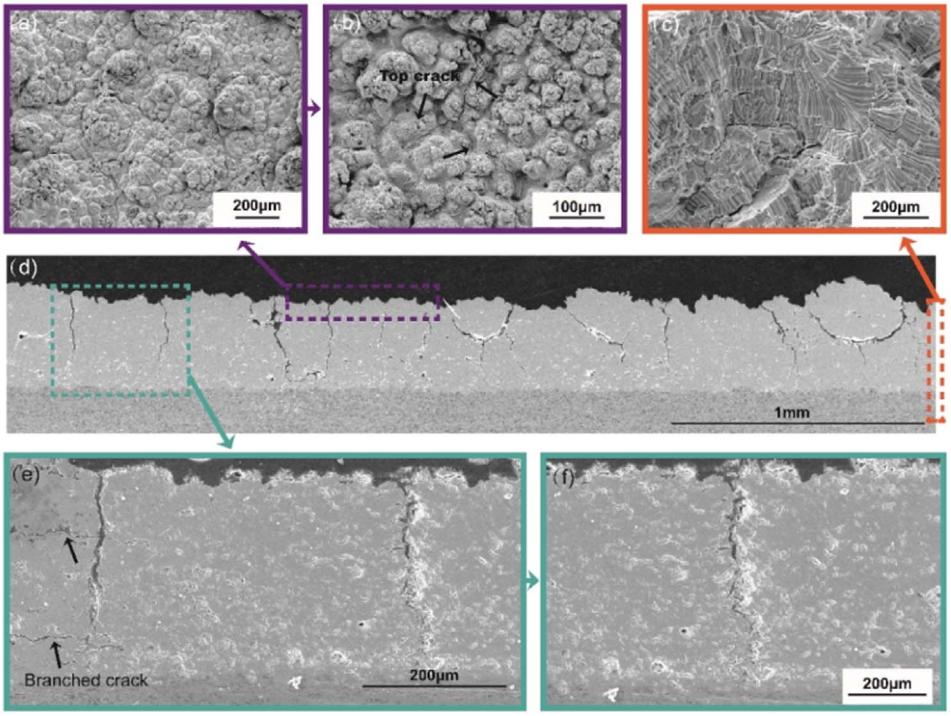

Fig. 8. Top surface (a, b), cross section (d, e, f) and fracture surface (c) of YSZ coatings at the spraying distance of 250 mm (Sample D).

c), aggregated at the tip of those island-protrusions, and embedded into the previously solidified droplets of YSZ powders. As a result, a mixed liquid and gas deposition was obtained onto the substrate.

In Fig. 9, at the longest spraying distance of 300 mm, the microstructure was also characterized by dense structure with certain intervals of vertical cracks on the transverse section and orderly distributed island-protrusions on the top surface. The thickness of one lamella was < 2.5 μm, as shown in the fracture sections (Fig. 9-f). Also, the width and density of vertical cracks (Fig. 9-d, e) were all lower than those of the former four samples.

According to the overall observation of the five samples, diverse intervals of vertical cracks were all detected on the cross sections of every coating. The initiation and propagation of vertical cracks were attributed to the thermal residual tensile stress during spraying process.

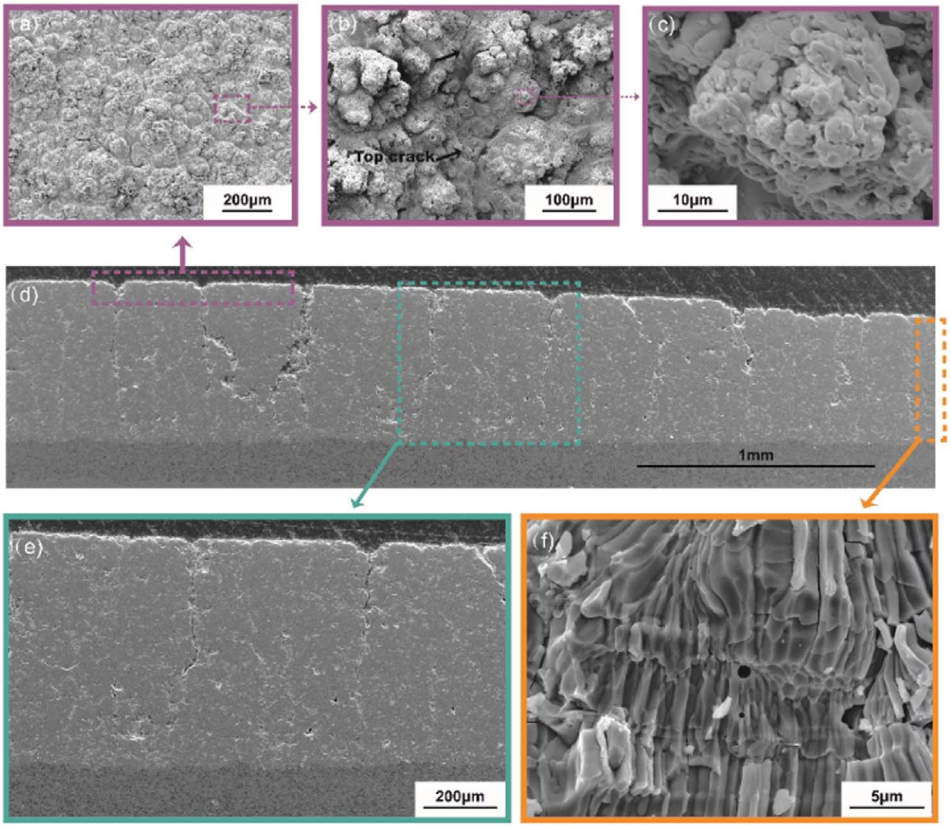

Fig. 9. Top surface (a, b, c), cross section (d, e) and fracture surface (f) of YSZ coatings at the spraying distance of 300 mm (Sample E).

During the cooling of droplets, thermal residual tensile stress was induced through the solidification constraint between the liquid droplets and the solid splat or the substrate. If the thermal residual tensile stress in the sample exceeds the adhesion strength between splats and the substrate and afterwards between the splats and the already deposited layers, horizontal cracks may propagate along the parallel direction of the coatings in order to release the tensile stress; on the other hand, if the thermal residual tensile stress in the sample exceeds the cohesion strength inside the coating, vertical cracks may propagate along the perpendicular direction [33]. Besides, the thermal residual tensile stress was intensely influenced by the substrate temperature [34]. The adhesion strength between splats was increased by epitaxial grain growth across adjacent splats at high temperature [35]. As a result, the density of transverse cracks was also increased with the increase of the substrate temperature, so that high crack density was achieved with high surface temperature and moderate pass thicknesses [36].

From the polished cross section views of the above coatings, the distribution of vertical cracks and their interval seemed irregular. However, by further focusing on the top surface of coatings, especially on the Samples B, C and D, it is seen that these vertical cracks were all segmented along the gaps between adjacent island-protrusions, which meant the accurate interval between adjacent vertical cracks was the diameter of every island-protrusion. The microscopic schematic diagram of the coating microstructure was demonstrated in Fig. 10. If the specimen is cut off and polished along the robot-scanning direction, namely, the radius direction of island-protrusions, identical intervals of cracks will be observed on the cross section of coatings, like in the cross-section observations of Samples C and E (Figs. 7 and 9). Based on the above results, the vapor deposited area on top of the coatings was intensely influenced by the spraying distance, a mass of vapor-deposited villous structures can be observed from the top surface of samples B and C (Figs. 6-c and 7-c) at the spraying distance ranging from 180 mm to 200 mm. This position represented the optimal melting condition that generated abundant villous structures during the spraying process and also affected the physical performances discussed in the following.

Fig. 11 demonstrated the single robot-scanning trace of the coating on the polished surface of the substrate at a spraying distance of 300 mm and scanning velocity of 0.6 m/s. The width of the single layer sprayed coating is about 5–7 mm, and also, the diameter of anode nozzle is 5 mm. The powders in the laminar plasma jet did not fly all over the substrate during the spraying process. It may provide a highly controllable thermal plasma spraying technology compared to the conventional plasma spraying equipment, especially for these smaller, complex and crucial components that need precisely deposited structures. Meanwhile, the merits of lower working noise, lower output power and controllability in laminar plasma spraying process provided a new selection of plasma materials processing and substantially improved the working environment of all workers.

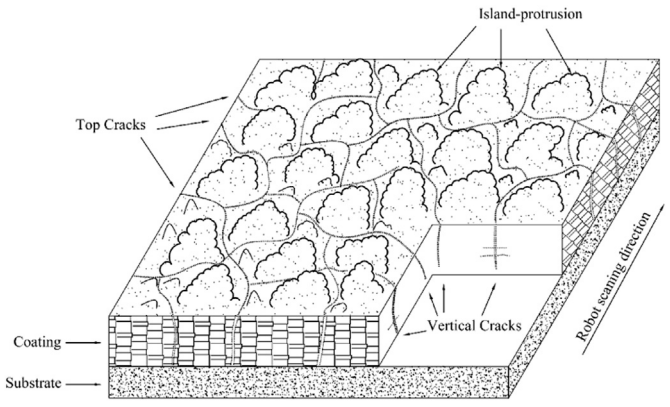

Fig. 10. Schematic diagram illustrating the microstructures of YSZ coatings.

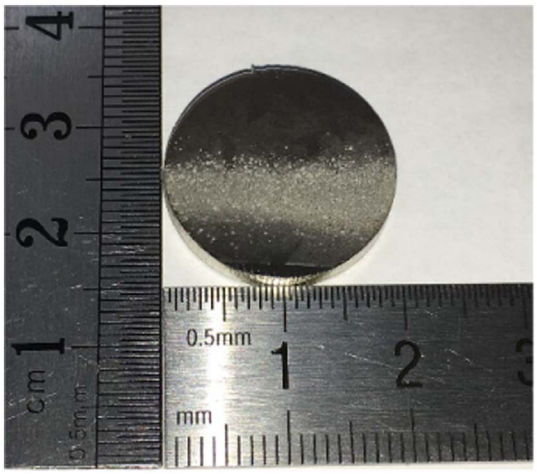

Fig. 11. Single robot-scanning trace of the YSZ coating on the polished surface of substrate at the spraying distance of 300 mm.

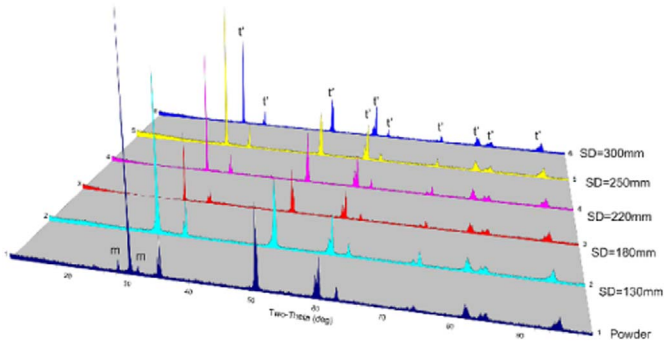

Fig. 12. XRD patterns of the plasma-sprayed YSZ coatings in comparison with the initial powder (t′-tetragonal ZrO_2; m-monoclinic ZrO_2).

4. Discussions of coating physical properties

4.1. Surface properties of the YSZ coatings

Fig. 12 shows the XRD patterns of laminar plasma sprayed YSZ coatings deposited at five different spraying distances in comparison with the initial powders. All the YSZ coatings presented the same phases as the powders. The porosities of samples C, D and E were lower than 4% (Fig. 13), but vertical crack areas were not considered in this measurement.

The cross-section hardness and top surface roughness of the above YSZ coatings were presented in Figs. 14 and 15. According to reference 37, the average hardness values of the SPPS and the APS coatings were determined to be 5.4 GPa (range 6.2–4.1 GPa) and 3.9 GPa (range 4.0–3.6 GPa), respectively [37]. The hardness values in the SPPS and APS coating were seen to be smaller than the one of the laminar plasma sprayed coating. Other Korean researchers worked on the 7%–8% yttria stabilized zirconia atmospheric plasma sprayed coatings of about 2000 μm thickness, the hardness values of the as-prepared TBCs with and without vertical type cracks were found to be 6.6 and 5.3 GPa, respectively [38]. The bulk hardness of the 7%–8% yttria stabilized zirconia is about 15 GPa. The surface roughness of the coatings in this study was quite higher than that of the atmospheric plasma sprayed or solution precursor plasma sprayed coatings.

4.2. Thermal conductivity of YSZ coatings

Thermal conductivity and thermal diffusivity are the most important thermo-physical material parameters for characterizing the

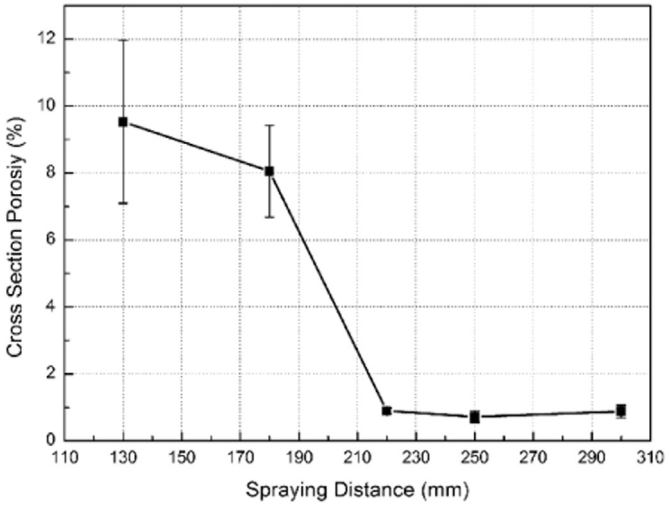

Fig. 13. Cross section porosity data of the coatings.

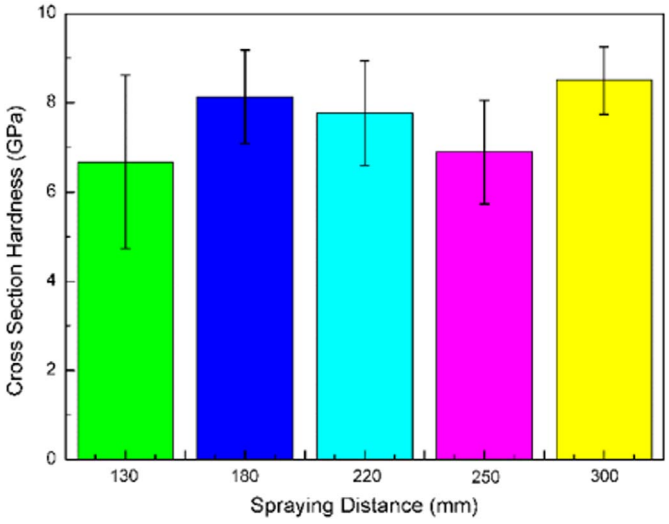

Fig. 14. Cross section hardness of the coatings.

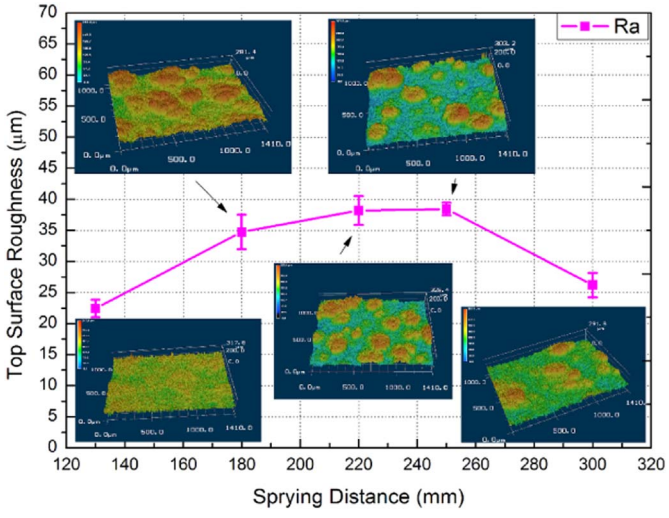

Fig. 15. Top surface topography data of the coatings.

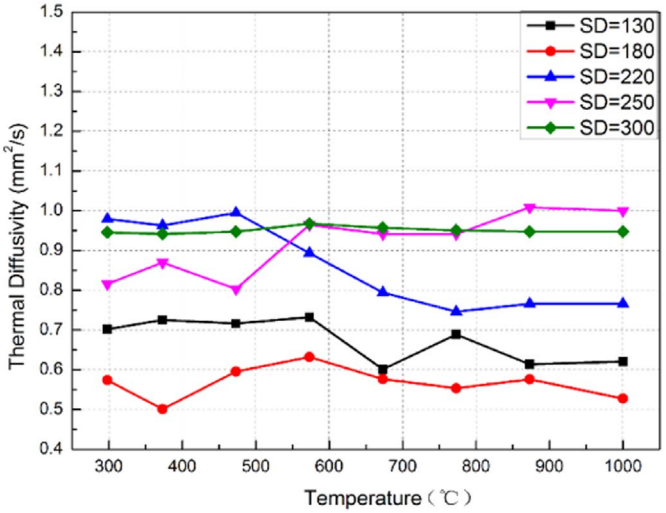

Fig. 16. Thermal diffusivity of the experimental YSZ coatings.

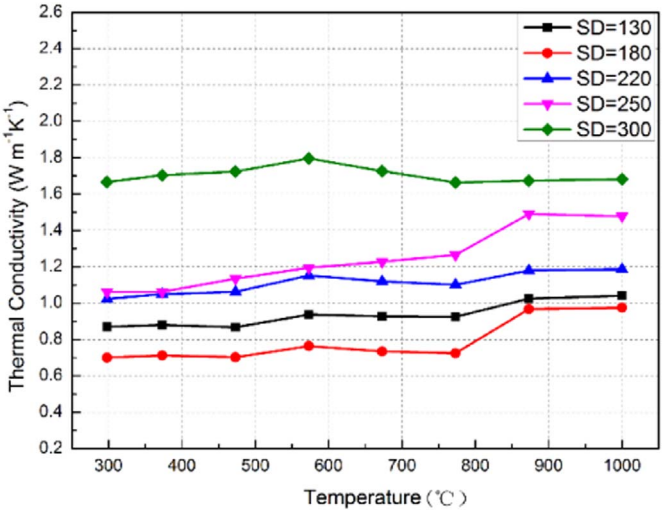

Fig. 17. Thermal conductivity of the experimental YSZ coatings.

thermal transport properties of YSZ coatings. Fig. 16 was mapped from the original temperature-dependent measured thermal diffusivity data of the laser flash technique. The thermal conductivities were calculated using Eq. (1) as shown in Fig. 17. Samples D and E with dense lamellar microstructure exhibited the highest thermal conductivity. The lower thermal conductivities were measured for Samples A and B due to their high porosity and crack density, which was closer to the level of the conventional APS coatings. The differences between the five samples can be principally related to the microstructures and porosities. It was evidenced from the above results that the vertical cracks and porous structure of the coatings can enhance the phonon scattering and reduce the phonon mean free path, leading to low thermal conductivity. Therefore, the porosity and the presence of vertical and horizontal cracks in the lamellar coating were recognized as vital factors in reducing the thermal conductivity.

5. Conclusions

The above results and discussions show that YSZ coatings can be deposited at super-long spraying distances ranging from 130 mm to 300 mm by laminar plasma jet at the conditions of output power of only 25–26 kW, gas flow rate of 14 L/min and working noise < 80 dB, which was quite unattainable through other conventional plasma spraying torches in atmospheric environment. Regular variation of

coating physical properties can be obtained by increasing the spraying distances, which means the melting state of particles also can be easily controlled through different spraying distances. Moreover, the refractory 8YSZ powder can be melted sufficiently in long laminar plasma jet, even up to the boiling point according to the top and polished sections of coatings, although the maximum output power of the laminar plasma torch is only 26 kW during the spraying process. Therefore, using this laminar plasma spraying equipment exhibits a promising potential for depositing advanced coatings, fundamentally improving the working environment of all workers and the controllability of the plasma spraying process.

Acknowledgements

The authors are grateful to Mr. Jing-Xi Wang from Department of Materials Science and Engineering in Xi'an Jiaotong University for the help in preparation of specimens. This work was supported by the Natural Key R&D Program of China (Basic Research Project, Grant No. 2017YFB0306100).

References

[1] O.P. Solonenko, M.F. Zhukov, Thermal Plasma and New Materials Technology Vol.1 Investigation and Design of Thermal Plasma Generators, Cambridge Interscience Publishing, 1994, pp. 5–43.
[2] P.L. Fauchais, J.V.R. Heberlein, M.I. Boulos, Thermal Spray Fundamentals, Springer Science + Business Media, 2014, http://dx.doi.org/10.1007/978-0-387-68991-3.
[3] E. Nogues, M. Vardelle, P. Fauchais, P. Granger, Arc voltage fluctuations: comparison between two plasma torch types, Surf. Coat. Technol. 202 (18) (2008) 4387–4393, http://dx.doi.org/10.1016/j.surfcoat.2008.04.014.
[4] P. Fauchais, Understanding plasma spraying, J. Phys. D. Appl. Phys. 37 (9) (2004) R86–R108, http://dx.doi.org/10.1088/0022-3727/37/9/R02.
[5] E. Pfender, Plasma jet behavior and modeling associated with the plasma spray process, Thin Solid Films 238 (1994) 228–241.
[6] V.I. Kuz'Min, O.P. Solonenko, M.F. Zhukov, Application of DC plasma torch with a quasi-laminar jet outflow, 1995 National Thermal Spray Conference, Houston, TX (United States), 1995, pp. 11–15.
[7] H.C. Wu, X.D. Yang, A Plasma Torch Used in Thermal Spray, CN2413467, 19990910, 1999. http://www.patent-cn.com/H05H/CN2413467.shtml, .
[8] K. Osaki, O. Fukumasa, A. Kobayashi, High thermal efficiency-type laminar plasma jet generator for plasma processing, Vacuum 59 (2000) 47–54.
[9] H. Hideki, W. Fuminori, T. Sunao, N. Tetsurou, Development of quasi laminar plasma DC torch, J. Jpn. Inst. Met. 4 (2001) 5–6 (in Japanese), https://www.jstage.jst.go.jp/article/jwstaikai/2011f/0/2011f_0_180/_article/references/-char/ja/.
[10] W. Pan, W. Zhang, W. Zhang, C. Wu, Generation of long, laminar plasma jets at atmospheric pressure and effects of flow turbulence, Plasma Chem. Plasma Process. 21 (1) (2001) 23–35.
[11] Y. Ando, S. Tobe, H. Tahara, M. Tokuyama, I. Oppenheim, H. Nishiyama, TiO_2 film deposition by atmospheric thermal plasma CVD using laminar and turbulence plasma jets, AIP Conf. Proc. 982 (2008) 612–617, http://dx.doi.org/10.1063/1.2897866.
[12] M. Khutsishvili, L. Kikvadze, H.-J. Hartfuss, M. Dudeck, J. Musielok, M.J. Sadowski, Spraying powder materials by the high-enthalpy laminar plasma flow, AIP Conf. Proc. 993 (2008) 423–426, http://dx.doi.org/10.1063/1.2909166.
[13] J. Tang, S. Li, W. Zhao, Y. Wang, Y. Duan, Development of a stable dielectric-barrier discharge enhanced laminar plasma jet generated at atmospheric pressure, Appl. Phys. Lett. 100 (25) (2012) 253–255, http://dx.doi.org/10.1063/1.4729818.
[14] J. Krowka, V. Rat, C. Chazelas, J.-F. Coudert, Pulsed laminar arc jet with synchronized suspension injection-spectroscopic studies, J. Phys. Conf. Ser. 550 (2014) 12020, http://dx.doi.org/10.1088/1742-6596/550/1/012020.
[15] J. Miao, D. Yu, X. Cao, Y. Xiang, M. Xiao, J. Yao, Experimental study on the characteristics of a miniature laminar plasma torch with different gas flow patterns, Plasma Chem. Plasma Process. 35 (5) (2015) 879–893, http://dx.doi.org/10.1007/s11090-015-9632-y.
[16] X. Cao, D. Yu, M. Xiao, J. Miao, Y. Xiang, J. Yao, Design and characteristics of a laminar plasma torch for materials processing, Plasma Chem. Plasma Process. 36 (2) (2016) 693–710, http://dx.doi.org/10.1007/s11090-015-9661-6.
[17] Jiang long Wang, Investments of Mental Rapid Manufacturing by Laminar Plasma Torch, University of Science and Technology of China, 2015 (M.D dissertation. In Chinese).
[18] O.P. Solonenko, H. Nishiyama, A.V. Smirnov, H. Takana, J. Jang, Visualization of arc and plasma flow patterns for advanced material processing, J. Vis. 18 (2014) 1–15, http://dx.doi.org/10.1007/s12650-014-0221-6.
[19] O. Solonenko, A.V. Smirnov, Advanced oxide powders processing based on cascade plasma, J. Phys. Conf. Ser. 550 (2014) 120–127, http://dx.doi.org/10.1088/1742-6596/550/1/012017.
[20] Hideki Hamatani, F. W. Development of laminar plasma shielded HF-ERW process-advanced welding process of HF-ERW3. In Proceedings of the 2012 9th International Pipeline Conference, 1–8.
[21] W. Ma, Q. Fei, W. Pan, C. Wu, Investigation of laminar plasma remelting/cladding processing, Appl. Surf. Sci. 252 (10) (2006) 3541–3546, http://dx.doi.org/10.1016/j.apsusc.2005.05.037.
[22] W.X. Pan, X. Meng, G. Li, Q.X. Fei, C.K. Wu, Feasibility of laminar plasma-jet hardening of cast iron surface, Surf. Coat. Technol. 197 (2–3) (2005) 345–350, http://dx.doi.org/10.1016/j.surfcoat.2004.06.043.
[23] Hideki Hamatani, OHARA, Masahiro, FUJI, Masao, development of high power hybrid plasma spraying, J. Jpn. Inst. Met. 63 (1) (1999) 135–143 http://ci.nii.ac.jp/naid/10002548732/en/ (in Japanese).
[24] Y. Ando, S. Tobe, H. Tahara, M. Tokuyama, I. Oppenheim, H. Nishiyama, TiO_2 film deposition by atmospheric thermal plasma CVD using laminar and turbulence plasma jets, AIP Conf. Proc. 982 (2008) 612–617, http://dx.doi.org/10.1063/1.2897866.
[25] M. Khutsishvili, L. Kikvadze, H.-J. Hartfuss, M. Dudeck, J. Musielok, M.J. Sadowski, Spraying powder materials by the high-enthalpy laminar plasma flow, AIP Conf. Proc. 993 (2008) 423–426, http://dx.doi.org/10.1063/1.2909166.
[26] W. Ma, W.X. Pan, C.K. Wu, Preliminary investigations on low-pressure laminar plasma spray processing, Surf. Coat. Technol. 191 (2–3) (2005) 166–174, http://dx.doi.org/10.1016/j.surfcoat.2004.02.011.
[27] B. Cheng, Y.-M. Zhang, N. Yang, et al., Sintering-induced delamination of thermal barrier coatings by gradient thermal cyclic test, J. Am. Ceram. Soc. 100 (2017) 1820–1830.
[28] Standard Test Method for Thermal Diffusivity by the Flash Method, E1461, ASTM, 2007. http://www.astm.org/DATABASE.CART/HISTORICAL/E1461-07.htm, .
[29] J. Parker, R.J. Jenkins, C.P. Butler, G.L. Abbott, Flash method of determining thermal diffusivity, heat capacity and thermal conductivity, J. Appl. Phys. 32 (1961) 1679–1684.
[30] Guangqi Liu, Ma Lianxiang, Jie Liu, The Manual of Chemical Property Data Inorganic Volume, Chemical Industry Press, Beijing, 2002, p. p255 (In Chinese).
[31] A. Jadhav, N.P. Padture, F. Wu, E.H. Jordan, M. Gell, Thick ceramic thermal barrier coatings with high durability deposited using solution-precursor plasma spray, Mater. Sci. Eng. A 405 (2005) 313–320, http://dx.doi.org/10.1016/j.msea.2005.06.023.
[32] M. Gell, E.H. Jordan, M. Teicholz, B.M. Cetegen, N.P. Padture, L. Xie, D. Chen, Thermal barrier coatings made by the solution precursor plasma spray process, J. Therm. Spray Technol. 17 (5) (2008) 124–135, http://dx.doi.org/10.1007/s11666-007-9141-5.
[33] L. Xie, D. Chen, E.H. Jordan, A. Ozturk, F. Wu, X. Ma, ... M. Gell, Formation of vertical cracks in solution-precursor plasma-sprayed thermal barrier coatings, Surf. Coat. Technol. 201 (3–4) (2006) 1058–1064, http://dx.doi.org/10.1016/j.surfcoat.2006.01.020.
[34] S. Sampath, X. Jiang, J. Matejicek, A. Leger, A. Vardelle, Substrate temperature effects on splat formation, microstructure development and properties of plasma sprayed coatings Part I: case study for partially stabilized zirconia, Mater. Sci. Eng. A 272 (1) (1999) 181–188, http://dx.doi.org/10.1016/S0921-5093(99)00459-1.
[35] C.J. Li, G.J. Yang, C.X. Li, Development of particle interface bonding in thermal spray coatings: a review, J. Therm. Spray Technol. 22 (2–3) (2013) 192–206, http://dx.doi.org/10.1007/s11666-012-9864-9.
[36] M. Karger, R. Vaßen, D. Stöver, Atmospheric plasma sprayed thermal barrier coatings with high segmentation crack densities: spraying process, microstructure and thermal cycling behavior, Surf. Coat. Technol. 206 (1) (2011) 16–23, http://dx.doi.org/10.1016/j.surfcoat.2011.06.032.
[37] A. Jadhav, N.P. Padture, F. Wu, E.H. Jordan, M. Gell, Thick ceramic thermal barrier coatings with high durability deposited using solution-precursor plasma spray, Mater. Sci. Eng. A 405 (2005) 313–320, http://dx.doi.org/10.1016/j.msea.2005.06.023.
[38] Z. Lu, M.-S. Kim, S.-W. Myoung, J.-H. Lee, Y.-G. Jung, I.-S. Kim, C.-Y. Jo, Thermal stability and mechanical properties of thick thermal barrier coatings with vertical type cracks, Trans. Nonferrous Metals Soc. China 24 (2014) s29–s35, http://dx.doi.org/10.1016/S1003-6326(14)63284-2.